



## Development of an innovative wireless power transmission model for marine applications

Umar Farooq<sup>1</sup>, Hajira Masood<sup>1</sup>, Jiropast Suakaew<sup>2</sup>, Kruawan Wongpanya<sup>3</sup> and Wanchai Pijitrojana<sup>1\*</sup>

<sup>1</sup>Department of Electrical and Computer Engineering, Thammasat School of Engineering, Thammasat University, Pathum Thani 12120, THAILAND

<sup>2</sup>Department of Integrated Engineering, Faculty of Engineering, Pathumwan Institute of Technology, Bangkok 10330, THAILAND

<sup>3</sup>Spectroscopic and Sensing Devices Research Group, National Electronics and Computer Technology Center (NECTEC), Thailand Science Park, Pathum Thani 12120, THAILAND

\*Corresponding author: pwanchai@engr.tu.ac.th

### ABSTRACT

The conventional wired charging system for ship-to-shore charging of underwater vehicles is prone to specific problems related to unreliable connection mechanisms and safety. The wireless charging system overcomes the danger of electrocution, as the power is transferred from the shore to the ship via electromagnetic induction instead of traditional ways of transferring AC power in the marine environment. This paper presents a novel system-level modeling and designing of wireless power transmission for marine applications. The proposed system comprises three main components: (a) a shore-side mobile transmitter (Shore-SMT), (b) an onboard static receiver, and (c) another ship-side mobile transmitter (Ship-SMT). The Shore-SMT and Ship-SMT, each consisting of a circular array of magnets, rotate in the vicinity of the receiver with a fixed circular variety of coils, resulting in voltage induction in the receiver coil. Consequently, the induced voltage in the receiver coil charges the onboard batteries. COMSOL® MULTIPHYSICS environment is used for the modeling and simulation of the proposed system using finite element method (FEM). The test cases simulate the individual and mutual rotation of the transmitters at several distances from the receiver coil. A prototype of the model is also developed. Experimental results from the developed prototype show promising performance as the percentage of transferred voltage increases from a single layer of x9 coil and x9 magnet bars to 70-75% and 80% in a double layer of x9 Ferro bars with x9 winding coils and double-sided x12 magnets and x9 winding coils respectively. It proves to be a better alternative to the conventional methods used for Ships and Vessel charging.

**Keywords:** WPT, Underwater vehicles, Wireless charging, FEM analysis

### INTRODUCTION

With the increasing development in wireless technology, power cords will soon become obsolete and past memory. The advancement in wireless power transmission (WPT) makes it a promising technology to implement in unsafe applications if exposed to electric power, such as coastal transportation systems (charging ferries). In marine applications, WPT has replaced conventional approaches to overcome existential problems such as dependence upon mechanical contacts or plugs and exposure to mechanical wear and tear. Furthermore, coastal ferries operate in a harsh and saline environment that can post challenging for electrical safety. Reliable mechanisms for the quick and automatic disconnection of the charging system are also necessary to ensure safety if the ferry urgently needs to leave the dock.

To avoid this hassle and other issues regarding the reliability of the charging system, wired charging setups are being replaced by wireless charging technology. Ferries are equipped with a series of batteries with high storage capacity. Ferries start receiving the wireless power to charge the onboard batteries as soon as they are docked, saving time while conventional connection setup is eliminated. However, safety is still a concern as a massive amount of AC power is transmitted from the transmitter toward the receiver in the presence of highly conductive fluid, water. In the last decade, many breakthroughs have been made in underwater WPT technology, such as model analysis, optimization design, impedance matching, etc. [1-3]. Several vital parts and control mechanisms, including power electronics converters, transformers, passive elements, plugs, interconnectors, and a charging energy management system, are used in the battery charging path from the shore to the onboard battery (EMS).

Several charging mechanisms have been introduced, including AC, DC, and wireless options. Additionally, the most recent commercial shore-to-ship charging interfaces have also been introduced [4]. However, all these methods have drawbacks and issues regarding performance efficiency, reliability, and damage control. To overcome problems mentioned above associated with conventional methods. Wartsila [5] is the world's first commercial ferry operating with batteries capable of high-power wireless charging, and the successful project represents an inevitable breakthrough in the evolution of plug-in electrically operated vessels. Using a wireless charger, power transfer can start instantly as soon as the ship is docked rather than waiting until the cables are connected; hence, 20% of the time is saved, which can be utilized for charging purposes. Moreover, they overcome the safety issues regarding the connections, and the maintenance needs are reduced since wear and tear to connection lines is eliminated.

In Norway, the government has promoted the accurate zero-emission operation of short-distance coastal transportation [5]. Thus, governmental development contracts have challenged the marine industry to develop technology for battery-based, double-ended ferries for short fjord crossings along state highways. As a result of successful technology demonstrations, many ferry routes in Norway are expected to be converted into fully battery-based or plug-in hybrid operations during the coming years. Industrial development enabling this transition toward zero-emission operations will likely find widespread applications worldwide. The significant advantage is 20 percent more utilization of the available charging time, improved operational safety, and increased system reliability.

In [6], the authors proposed an elaborate analysis of the underwater Wireless Power Transmission system (inductive power transfer) and figured out an effective method for tracking the maximum power efficiency. In [7], the authors designed a WPT system for Autonomous Underwater Vehicles (AUVs) and transmitted a charging power of 300W, attaining an efficiency of 75% to 91%. In [8], the researchers contributed to reducing the receiver size and maintaining a constant current by studying the inductor-capacitor-capacitor and parallel (LCC-P) compensated WPT system. A unique, three-phase WPT structure having acceptable eccentricity resistance was developed and analyzed in [9], transferred 1.0 kW with an efficiency of 92.41%. Nonetheless, the Inductive Power Transfer (IPT) technology has some restrictions on being directly applied in the water due to the large amount of eddy-current loss induced by the high-frequency magnetic fields [10].

This paper uses a novel and safe method to transmit the voltage in the marine environment to charge the electric vessels. The proposed model is designed and simulated in the COMSOL MULTIPHYSICS software, and transmitters and receiver coils are created and performed as a complete system. The model can be tested for real-time function by simulating different scenarios. It is tested for three significant cases to achieve the best possible efficiency. Then, a prototype is built, experiments are performed in real-time, and the experiments and simulation results are compared. The rest of the paper is organized as follows. In Section 2, related work is discussed. In Section 3, the overview of the proposed method is discussed. In Section 4, a performance analysis of the proposed system is conducted, and various simulations performed are discussed. In Section 5, experimental results are examined, and the paper ends with a conclusion and discussion of results, acknowledgment, and references in the last sections.

## MATERIALS AND METHODS

Optimization frequency in the IPT system can be attained by analyzing and considering the Eddy Current Loss (ECL) in an underwater WPT system [10]. To reduce the ECL of the underwater WPT system, an  $A1 \times 1 \times 1$  structure was proposed, which also improved AC-AC power transfer efficiency by nearly 10% compared to the conventional [11]. In [12, 13], researchers optimized the wireless power transmission coils and the operating frequency by analyzing the EMF around the underwater WPT system. Besides, using ferrite cores can enhance mutual inductance, and thus, ECL can be decreased. However, the IPT system usually requires a relatively complicated coupler structure [14], including coils, ferrites, and shielding, which is difficult to seal in the water environment. Therefore, it is challenging to apply IPT technology to charge underwater devices.

On the contrary, Capacitive Power Transfer (CPT) technology is a better technique to charge the devices in the underwater environment and on the water's surface [15-16]. All three main limitations of the IPT system could be countered by the CPT technique [17]. Instead of magnetic fields, high-frequency electric fields are used for power transmission, so eddy current loss (ECL) will be eliminated. The capacitive coupler only needs metal plates, which can be easily sealed and are immune to the high pressure in the underwater environment. The CPT underwater shore-to-ship charging systems can be categorized into three categories: (1) Conductive, (2) Wireless, and (3) battery swapping. The conductive connection to the charging station of the electric vehicle is made via charging plugs classified

as AC and DC types and robot arms. The AC connector type 1 category has only single-phase functionality, and this type of connector is mainly used in home-charging Electric Cars. A different kind of AC connector, also known as Mennekes, after the manufacturer of this design, supports both single- and three-phase connections and is mainly used in the EU. This type of charging falls into the slow or semi-fast category. Thus, the electrocution process through a cable management system is less reliable and safe but more complex. Battery swapping is another solution for the CPT underwater shore-to-ship battery charging system.

The entire process takes much less time than fast or ultra-fast charging methods. In the case of EC, the current situation is that it is challenging to introduce it because the capacity and shape of the battery and how to incorporate it into EC differ for each EC brand. It will only be possible and advantageous if the way batteries are attached to the EC is standardized and companies can follow standards based on it. On the other hand, in the case of Electric Ships (ESs), especially ferries, battery replacement is very convenient and profitable. The ferry's waiting duration is short. Hence, spare battery packs can be stored at either or both ends depending on whether the ferry route is short or long for the journey. Also, ferry operations are limited to one specific route, which is a plus for using this technology. This way, ferry and inland freighter operating hours and trips can be extended. However, with the battery swapping system, there are effectively more batteries for the same number of EVs and ESs, putting more strain on a limited pool of resources. Removable batteries also suffer from short operating distances due to their disposable nature. The wireless charging system is a reliable alternative to conductive and battery swapping in the CPT system. EV charging can be categorized into slow, semi-fast, fast, and ultra-fast types, but the main challenge is the charging time to charge the onboard battery, which typically takes minutes to hours. Several optimized approaches are being pursued to minimize charging time comparable to gasoline refueling times.

A better and more advanced approach, Floating Charging Stations (FCS), has also been introduced. Electric charging stations, a novel idea, along the marine routes. Due to its complete isolation from the traditional electric grid and its built-over, especially floating platforms, the offshore FCS should be self-sufficient with storage options [18]. However, direct access to the charging station may compromise the integrity of the floating platform structure that the charging station is built over in the event of massive vessels. Additionally, ships approaching the station may only

sometimes be able to veer from their voyage route to access the FCS directly if the charging stations are slightly distant from the sea route [20]. The super-capacitors push a lot of current to the load during early charging, making that process faster. As time passes, the batteries will support the charging at average speed.

### *Proposed system*

As mentioned in Figure 1(a), the constant current (CC) method is pursued in conventional methods. A constant current is maintained throughout the charging process based on the State of Charge (SoC) with an onboard battery pack. The advantage of this technique is that the current supplied throughout the process is limited, and the charging current can be easily determined. The main drawback is that the battery pack may overcharge every time the SoC estimation algorithm fails, ultimately shortening battery life. Battery charging rate is defined by the C rate, which indicates the rate at which the battery is charged or discharged. Here, a 1 C charge is a battery charging in 1 hour. An increase in the C-rate, essential for ultra-fast charging, leads to increased heat generation, which ultimately impacts lifespan if adequate cooling is not guaranteed. Also, coupling capacitance drops significantly when the distance is increased. Moreover, in the conventional approach, when the ship is docked on the shore, it keeps moving up and down in the water, leading to a misalignment between the transmitter and receiver. Besides, high-frequency excitation voltage is transferred by the transmitter (Tx) to the receiver, which is merged into the water. There is a high risk of electrocution during the transfer of power. The conventional and proposed methods used for charging purposes are depicted in Figure 1(a) and (b).

This paper proposed an innovative approach to overcome all the problems regarding reliability, time, safety, and complex structures. The proposed research also provides a solution for charging the batteries during the journey without the hazard of electrocution. To overcome the problems related to the current conventional CPT shore-to-ship charging system, it is replaced with a wireless charging system, as illustrated in Figure 1(b). There are two transmitters in the proposed system: the shoreside mobile transmitter (SMT) and the ship-side mobile transmitter rotating in the vicinity of the receiver. These are an array of magnets that result in the induction of voltage in the receiver coil. Consequently, voltage is induced in the receiver coil, which is utilized to charge the onboard batteries. Since there is no high AC voltage transmitted by the transmitters, unlike traditional transmitters, there is no risk of high input voltage in the marine environment. The rotation of the transmitters, one on



top and one on the bottom, results in voltage induction in the coil, which is then further processed (stepped up or down) and used to charge the onboard batteries.

The system is insulated with insulation, blocking the hazard of electrocution on the vessels.

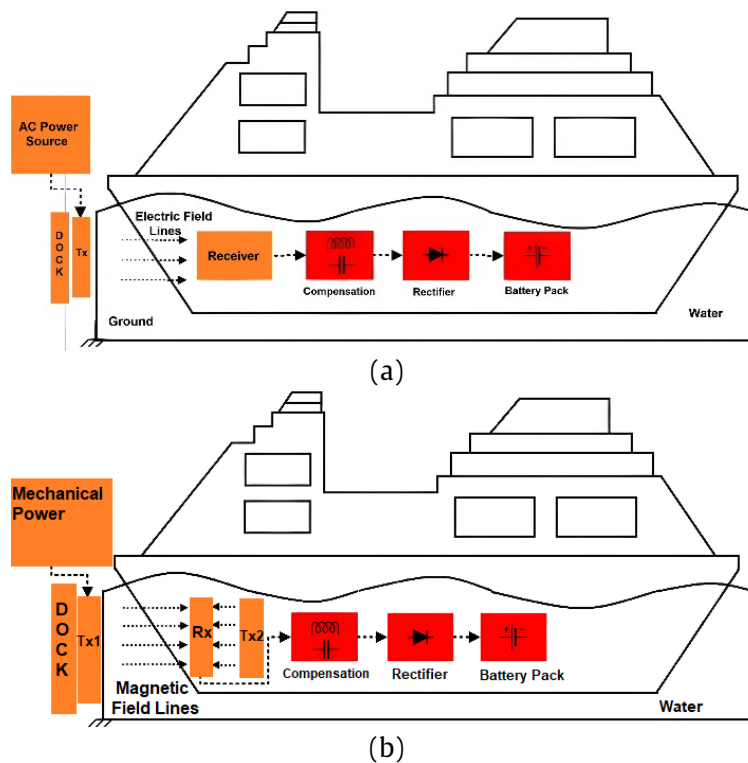


**Figure 1** (a) Conventional charging system (b) Proposed system in marine environment.

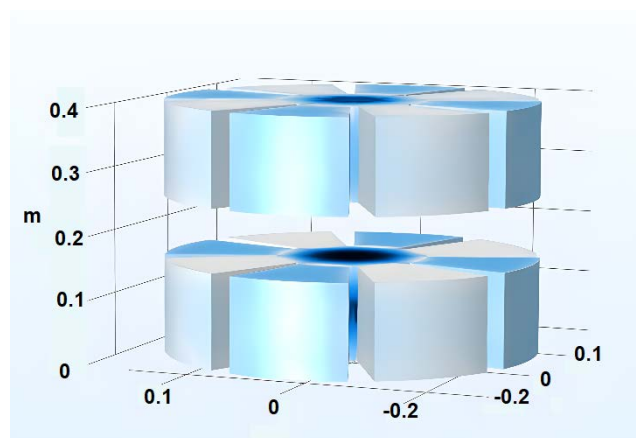


**Figure 2** Representation of segmented geometry of transmitters.

For the modeling of the proposed system and simulation in a finite element environment, the COMSOL® MULTIPHYSICS environment is chosen. The proposed model involves simulating the flux density distribution employing rotating transmitters. The overview of the proposed model is shown in Figure 2. The system is insulated with insulation, blocking the hazard of electrocution on the vessels. The simulation domain is the rotating domain that makes transmitters' magnets rotate. Consequently, the coil generates and receives the changing magnetic flux, and the voltage is induced inside the coil. For this purpose, built-in operation Rotatory Machines and magnetic physics are utilized.

The magnetic field of a magnetic dipole moment vector ( $m_1$ ) can be written as [19].

$$\vec{B}_{dip}(\vec{r}) = \frac{\mu_0}{4\pi} \frac{1}{r^3} \left[ 3 \left( \vec{m}_1 \cdot \frac{\vec{r}}{r} \right) \frac{\vec{r}}{r} - \vec{m}_1 \right] \quad (1)$$

The magnitude of the field is directly proportional to the magnitude of its dipole moment, inversely proportional to the cube of distance ( $r$ ), where ( $\mu_0$ ) is the permeability of free space. The magnetic dipole moment is proportional to the volume of a magnet ( $V$ ), and the residual magnetic field ( $B_r$ ) of the magnet is expressed as:

$$\left| \vec{m}_1 \right| = \frac{VB_r}{\mu^o} \quad (2)$$

Due to the field ( $B_{dip}$ ) created by each rotor, there is a torque described as the twisting effect that tends to align the dipole in the direction of that field, as shown.

$$\vec{T} = \vec{m}_2 \times \vec{B}_{dip} \quad (3)$$

where  $m_2$  is the magnetic dipole moment vector of the magnet of the receiver side. The mechanical power transferred ( $P_m$ ) is the product of the torque ( $T$ ) and the angular frequency of rotation ( $\omega$ ) and is written as:

$$P = \omega T \quad (4)$$

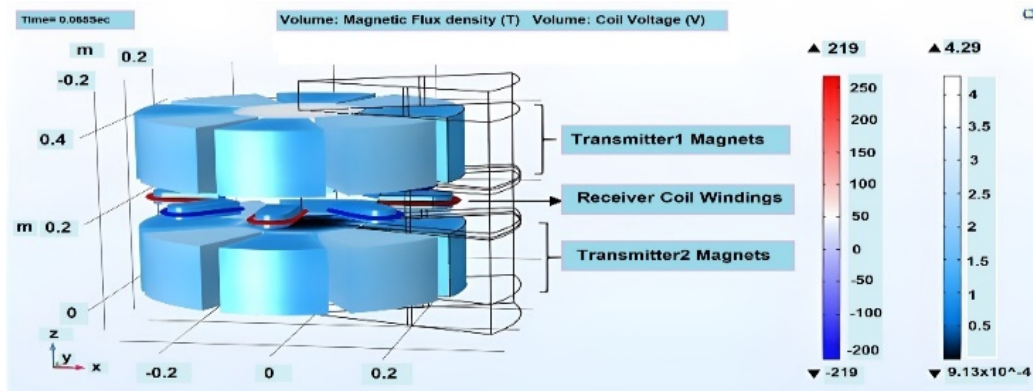


**Figure 3** Overview of the Proposed Model.

### *Shore and ship-side mobile transmitters (array of magnets) design*

A circular array of magnets is constructed using the physics of rotating machinery, magnetic (mm), to model the transmitters. Both landside and shipside transmitters are the same size and have the exact dimensions. Manufactured with permanent magnets called N50 (Sintered NdFeB), a rare-earth magnet, the dual rotary transmitter is designed for maximum torque-to-weight ratio. A circular array of eight magnets is created by constructing each magnet into a sector using the following sector angles: 45 degrees for each, making it 1/8th of the total geometry containing the magnets, coil, and soft iron in each sector. In the traditional approach, the distributed coils are only partially active as they overhang the magnets. The sector model approach avoids this because overhangs add weight, cost, resistance, and heat. This model has a fan-shaped arrangement of the transmitter magnets and coils, resulting in a fully active winding design with much less coil overhang. The design is, therefore, compact and small, and the reduced weight increases the magnetic flux area to generate more power. For each sector, a base geometry sketch is created using SOLIDWORKS. It is imported in COMSOL, and an

Equation (4) shows the power transferred between the transmitter and receiver through the air gap. Another essential factor to consider is that the magnetic insulation boundary must be set so that no flux is leaked. Another crucial factor to consider is that the magnetic insulation boundary must be fixed so that no flux is leaked. Modeling and analyzing are performed in three steps; firstly, the rotating transmitter with a central coil is modeled, and the results are interpreted. Secondly, one rotating transmitter is halted, and simulation is computed. Finally, rotating transmitters are moved away from the coil, and simulation is carried out for different distance proximities. The design of each component of the system is explained in detail below.

intersection operation is performed to retain a magnet and rotor iron sector. This geometry is then rotated at an angle of -22.5 to reorient it in the domain and extruded to form a sector that contains the rotator iron core, as shown in Figure 2 and 3. The rotor is enclosed in air by extruding a fluid domain below. A fluid domain above is formed, which contains the coil and soft iron core, and then the rotor below is mirrored up to obtain the two rotating magnet sectors. Also, a soft iron core is extruded for the coil. This forms our complete rotating domain sector, along with two magnets enclosed in air and iron.

Each sector is combined to form an entire solution for the complete geometry, as shown in Figure 4. Ampere's law is applied to each industry of magnets where the magnetic strength is defined for the magnets as 1.4T. The geometric parameters of the proposed system are illustrated in Table 1. The relation between field variable magnetic field intensity and electric current density, magnetic flux density and area, and electric field and electric current density are shown in equations (5), (6), and (7).

$$\nabla \times H = J \quad (5)$$

$$B = \nabla \times A \quad (6)$$

$$J = \sigma E \quad (7)$$

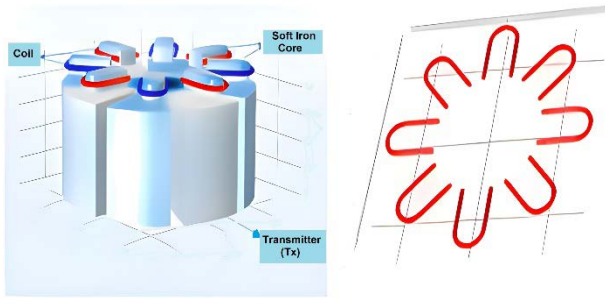


**Figure 4** Representation of the entire receiver coil geometry.

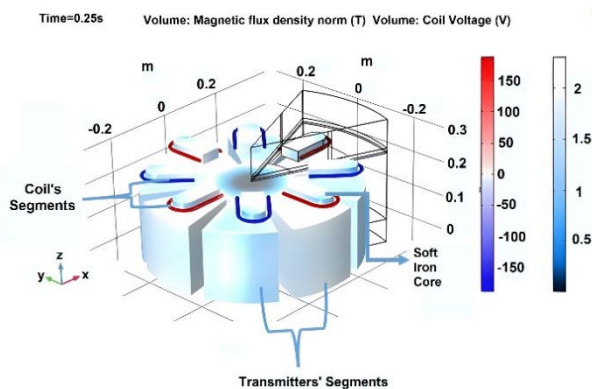


**Figure 5** Segmented geometry of Coil and a Transmitter.

**Table 1** Geometric parameters of the simulated system in COMSOL.

Parameters	Values
Radius	1 m
Sector angle	45
Main construction plane	XK
Space dimensions	3
Number of domains	11
Number of boundaries	72
Number of edges	142
Number of Vertices	82
Transmitter 1 domain Thickness	0.165
Transmitter 2 domain Thickness	0.01

With the sector model approach, computing time is optimized not only for the shape of the magnets and their proximity and relative motion to the coil, which are optimized to get a better value of sinusoidal voltage. Before using the sector model approach, a crude design to start the problem consisted of 2 rotating disks surrounding a large circular single coil in between. The magnet size and alignment with the coil were not optimized; a soft iron core was needed to help the coil strengthen the magnetic field. After the simulations, the voltage was achieved at the end, but the curve was not smooth and had many voltage fluctuations. Many conditions were overlapping, leading to an incorrect solution, which is why the voltage induced initially resolved to zero over time, and convergence was moving towards singularity. Moreover, results were

inconsistent as the Magnetic field was unevenly distributed in the domain due to a large circular copper disk, and the voltage curve was unevenly distributed over time and was staggering. Resultantly, the compute time is more than 12 min per single run, even with simplified Solver settings and low-resolution mesh. Hence, sectors were made for all the components with a sector angle of 45°, making it 1/8th of the total geometry containing each sector's magnets, coil, and soft iron. The solution solved for each industry is combined in the result field to form an entire solution for the complete geometry, significantly decreasing the computing cost. With the new sector model, not only was compute time optimized, but in the new model, the shape of the magnets and their proximity and relative motion to the coil were optimized to get a suitable voltage sinusoidal profile and the most decisive factor in obtaining a significantly better voltage profile of magnets. The new computing time per several iterations and method of termination shown in Table 2 for the sector model was just over 2 minutes, even though the model domain, Entities involved, and conditions were complex compared to our previous model. The results of our new improvised model are given below.

**Table 2** Method and termination.

Description	Value
Termination technique	Iterations or tolerance
Number of iterations	15
Tolerance factor	100
T	range (0,1/50,1)*1/60[rpm]/4
Timestamp	2.5E-4[s]

### Receiver coil design

The receiver coil is also designed using the sector model approach to achieve concentrated voltage with low losses, less weight, and no coil overhangs. To design the receiver coil, a circular surface with a diameter of 5 mm is defined in the yz plane, and then a path is created along the x-y plane as a homogenized multi-turn conductor.

The single coil has a U-shape, and multiple turns with coil conductivity  $6 \times 10^7$  [S/m] are selected by clicking on it and choosing from the settings box. The rest of the properties specified for the coil segments can be seen in Table 3 below. The circular coil is then swept across that path using the sweep feature of COMSOL. Like transmitter construction, a single coil section is modeled, and its alignment with the magnet size is optimized. A soft iron core around which the coil is wound strengthens the magnetic field. The individual coils are designed on an xy plane with a z-coordinate of 0.197 and placed 45 degrees apart, as



shown in Figures 4 and 5. These coil sections between the transmitter sections are joined to form a complete geometry and make it work properly. Each coil section is placed between the transmitters so that the magnetic flux variation influences it.

**Table 3** Parameter and Values of Coil.

Parameters	Values
Number of turns (N)	100
The diameter of the wire in the winding	0.001 m
Area (A)	$7.9e - 5 \text{ m}^2$
Coil wire conductivity	$6 \times 10^7 \text{ [S/m]}$
Coil current	30 [mA]
Coil length multiplication factor	17
Coil area multiplication factor	1

Equations for coils on top of moving magnets are as follows: (1) Ampere's law

$$\nabla \times B = \mu_0 J$$

$$\nabla \times H = J$$

$$J = \sigma E$$

1) Magnetic insulation 1

$$n \cdot B = 0 \quad (8)$$

2) Magnetic flux conservation: Air domain lowe

$$\nabla \cdot B = 0$$

$$B = \mu_0 r H \quad (9)$$

$$H = -\nabla V_m$$

3) Magnetic flux conservation: Rotor iron

$$H = -\nabla V_m \quad (10)$$

4) Periodic condition for coils

Vector potential formulation (Ampere's law)

$$A_{src} = -A_{dst} \quad (11)$$

Scalar potential formulation (Magnetic flux conservation)

$$V_m.src = -V_m.dst \quad (12)$$

### Performance analysis

The finite Element Method is adopted for geometry with more than one dimension because the results are then a grid of a basis function. In the proposed system, the physics-controlled mesh is applied for the overall model, while a separate "Moving Mesh" is defined for the rotating parts of the system, i.e., Transmitters. The accuracy of the solution in FEM depends on the density of the mesh, which is interrelated to the computational cost. An accurate solution may

result in a very high computation cost. The software allows the user to pick the order of element discretization for each dependent variable. However, the degree of freedom increases with the increment in element discretization. Consequently, the computational time is increased, and it takes longer to solve, especially for time-dependent problems. In the proposed system, since the transmitters and receiver have some structured geometry, the structured mesh is preferred, as shown in Figure 6. Additionally, the physics of the model is known; therefore, its physics-controlled meshing option is selected. The Sectional geometry of a single coil loop can be seen in Figure 7.

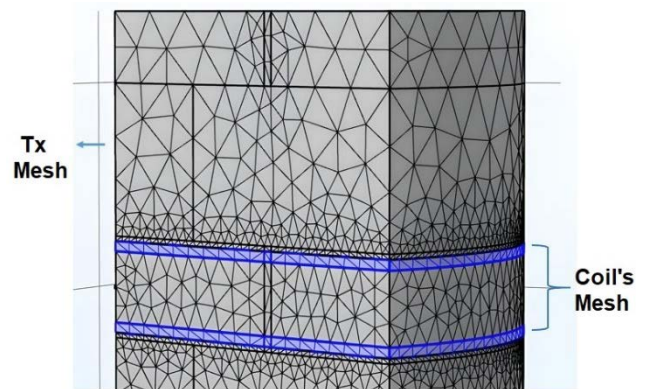


**Figure 6** Complete Mesh Structure of a Coil and a Transmitter's Segment.

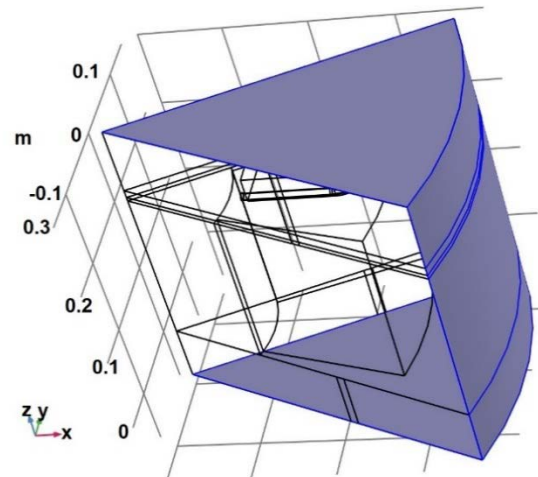


**Figure 7** Representation of coil sectional geometry.

After completing mesh analysis, various simulations are carried out to evaluate the model's performance and determine the value of voltage induction and transmitted power in the receiver coil under multiple circumstances. All the cases are explained in detail below.

### Case 1: Simulation with both transmitters rotating

To analyze the work performance of the model, three different simulations were carried out with other parts of the model in operation. In the first case,

both transmitters are kept 5 cm from the receiver coil and rotated with an rpm of 100. The number of turns of the receiver coil is considered 100 throughout the simulation. Each coil sector is aligned with the sectors of the magnets (as shown in Figure 8a) so that the maximum flux passes through the air domain with the rotation of both transmitters. In this case, the wire resistance is not ignored, and even though the rpm value still needs to be high, it gives promising results. The magnetic flux lines generated by the rotation of transmitters are highlighted and shown in Figure 9.

As shown in Figure 10, the total voltage induced in the receiver coil is around 270 V. As expected, the flux density is higher when both transmitters rotate simultaneously near the receiver coil wire, thus causing more voltage.

### Case 2: Simulation with one transmitter rotating

In this case, the top transmitter is fixed, and only the lower transmitter rotates. The rpm of the rotating transmitter, its distance from the coil, and the number of coil turns are about their previous values. The magnetic flux density is now weak, as depicted by flux lines in Figure 11, and the induced voltage is reduced to half of the original with both transmitters rotating, as shown in Figure 12.

However, as there is a direct relation between the induced current and rpm, increasing the rpm will increase the induced current; similarly, increasing the number of turns in the winding can improve the voltage value.

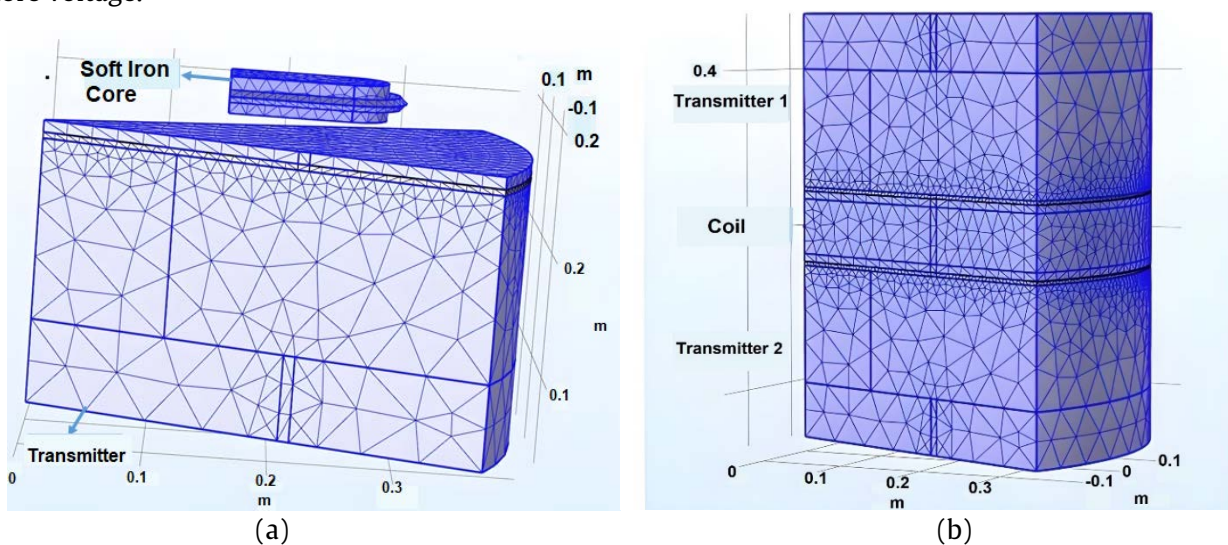


**Figure 8** (a) shows the shore-SMT and Receiver Coil Winding, and (b) shows the Receiver coil between the Shore and ship-SMTs.

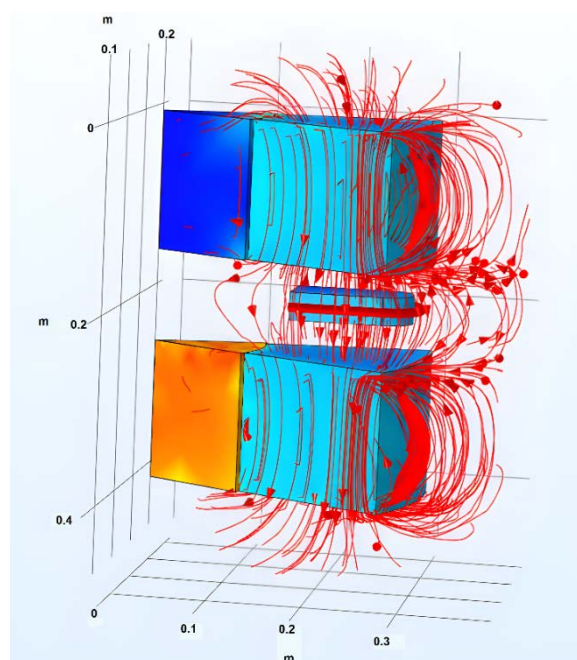


**Figure 9** Magnetic flux lines and field generated by the rotation of both transmitters.



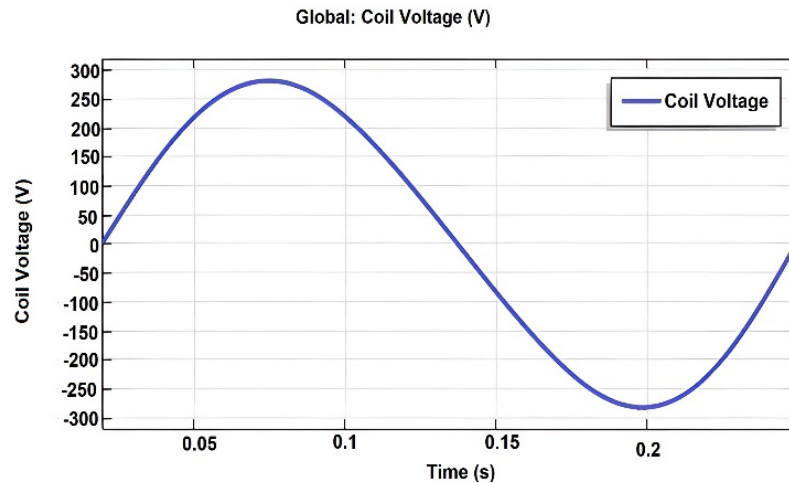


**Figure 10** Voltage induced in the receiver coil (Case 1).

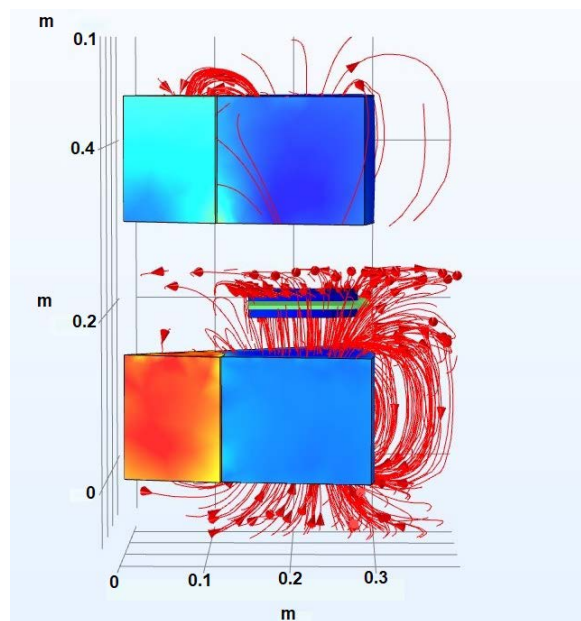


**Figure 11** The rotation of a single transmitter generates magnetic flux lines and fields.

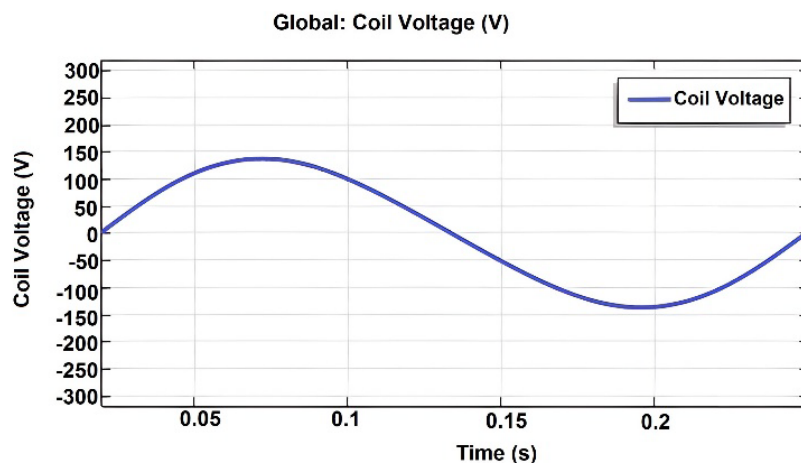


**Figure 12** Voltage induced in the receiver coil (Case 2).

*Case 3: Simulation with changing transmitter position*

In this case, the position of the rotating transmitters varies from 5 cm to 7 cm, as shown in Table 5. Since the value of induced voltage is proportional

to the magnetic flux passing through the receiver coil from the rotating transmitters. The higher the flux value, the more voltage is generated in the coil. The relative distance of transmitters from the receiver coil

is essential in determining the value of induced voltage. From Table 4, the induced voltage in the coil decreases when the distance between the transmitter and receiver coil is increased. However, the voltage value is improved if the transmitters are moved away but rotated simultaneously.

The maximum voltage of 140 V is obtained at the transmitter's distance of 5 cm from the coil when one transmitter is kept static, and the other is rotated. Similarly, as the rotating transmitter is moved further apart at distances of 6, 6.25, 6.5, and 7 cm, the induced voltage decreases to 108.99, 103.33, 98, and 89 volts, respectively.

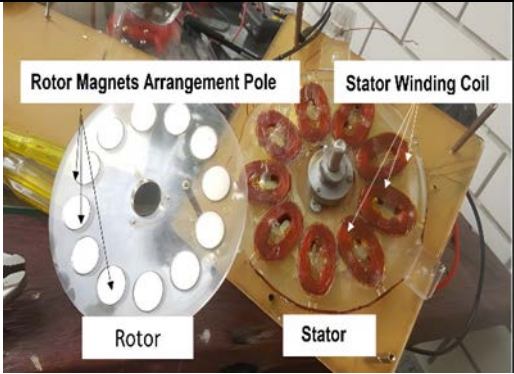
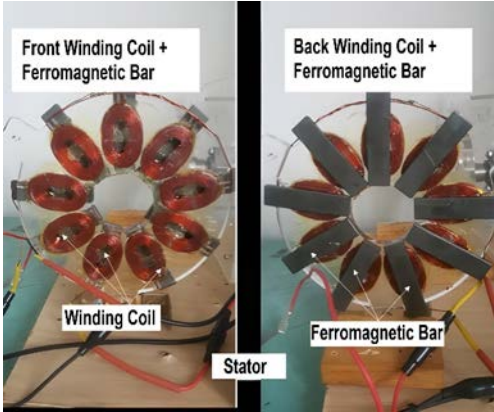
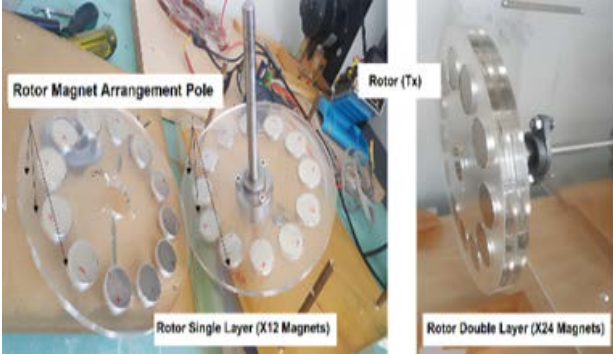
In the other case, when both transmitters are rotated, the maximum voltage of 280 V is induced with 5 cm between the coil and transmitters. Increasing the distance to 6, 6.25, 6.5, and 7 cm reduces the voltage

to 227.9, 208.34, 198.07, and 179.83 V, respectively. The distance of both transmitters affects the voltage value; however, if both are rotated simultaneously, the voltage rises.

**Table 4** Table of simulation with changing transmitter position.

Transmitter 1	Transmitter 2	Distance of	
		T1 from coil (cm)	T2 from the coil
Static	Rotating	5	5
Static	Rotating	5	6
Static	Rotating	5	6.25
Static	Rotating	5	6.5
Static	Rotating	5	7
Rotating	Rotating	5	5
Rotating	Rotating	6	6
Rotating	Rotating	6.25	6.25
Rotating	Rotating	6.5	6.5

**Table 5** Experimental Setup.

Module	Illustration	Description
Rotor and Stator		Rotor: Single layer (x12 magnets) Stator: Single layer (x9 winding coils)
Stator		Stator: x9 winding coils + x9 Ferro-bars
Rotor		Rotor: single layer (x12 magnets) double layer (x24 magnets)

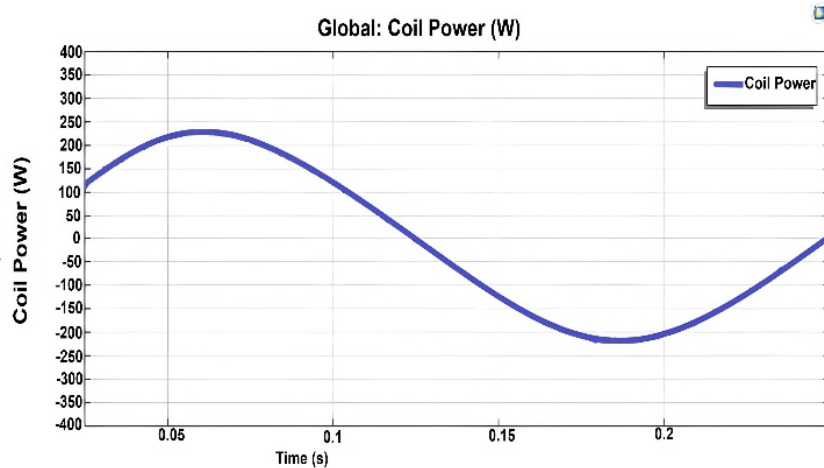


**Figure 13** Power generated in the coil.

### Transmitted power

The instantaneous power values can be accessed by the environment variable Coil, which is the coil power. Mathematically, simple power is obtained by taking the product of the instantaneous voltage of the coil and the instantaneous current through the coil. As the voltage is produced as a function of time during the rotation of the transmitter, the instantaneous voltage and resulting current are utilized to calculate the power, as shown in equation (13) below. The power when both transmitters are rotating at an rpm of 100, at 5 cm from the receiver coil, is described in Figure 13.

$$P(\text{coil}) = V_{\text{inst}} \times I_{\text{inst}} \quad (13)$$

## RESULTS AND DISCUSSION

### Experimental set-up

An axial flux permanent magnet topology, as shown in Figure 14 (a) single-side, (b) double-side, is used in the experimental setup. The magnets are designed and arranged so that the magnetic field of the individual magnets adds up to give the total field. Similarly, the coils are designed in such a way that maximum power is transferred, and magnetic flux leakage is reduced. Various simulations are carried out, and the amount of magnetic flux passing through the receiver coil for each simulation varies, resulting in different values of induced voltage. The experimental setup of hardware used for conducting the experiments according to simulation is shown in tabular form in Table 5. Many possible patterns exist between single-side and double-side topologies with the Tx rotor and the Rx stator. Still, this research studies the TX surface-mounted permanent magnet rotor patterns with the Rx surface-mounted winding coil stator. The single-side topology consists of one rotor and one stator. Two

rotors and one stator or vice versa illustrate the double-side topology.

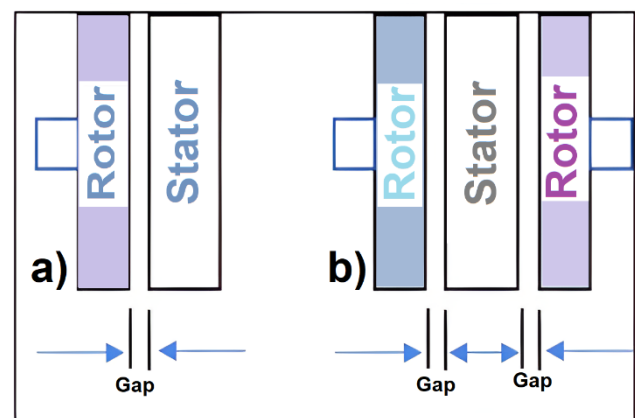


**Figure 14** a) Single-side permanent magnet topology. b) Double-sided Axial flux permanent magnet topology.

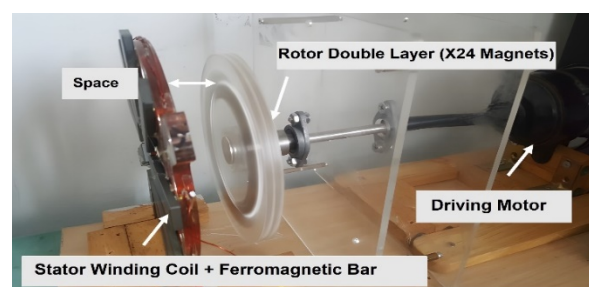


**Figure 15** Rotating magnetic transmitter and static coil experimental setup.

### Experimental results

This section presents the experimental analysis of the proposed, designed prototypes. Three prototypes of the proposed design have been developed using various coil sets with multiple turns in the stator plate and varying numbers of magnets in the rotor plates with different spacings. The prototypes are tested for multiple cases, and the resulting voltage, power, and current variations generated with the varying rpm are noted. The experimental setup is shown in Figure 15,



which includes a driving motor and an oscilloscope with a 2-channel probe for AC power measurement. The magnetic rotors (transmitters) were driven with the help of a driving motor so that both layers were rotated together on the same side in proximity to

the static winding coil. The driving motor rated at 75 W and operating at 700 rpm was designed using the same procedures, while the study patterns with Tx surface-mounted permanent magnet rotor and Rx surface-mounted winding coil stator are in Table 6.

**Table 6** Measurement results of Tx and Rx topology.

Topology	Rotor Module	Stator Module	Gap (cm)	System efficiency (%)
Single side	Single layer (x12 magnets)	Single layer (x9 winding coils)	0.5 cm.	50%
			1 cm.	40%
			1.5 cm.	30%
			2 cm.	10%
		Single layer with Ferro bar (x9 windingcoils + x9 Ferro-bars)	0.5 cm.	55%
			1 cm.	45%
			1.5 cm.	35%
			2 cm.	15%
	Double layer (x24 magnet)	Single layer (x9 winding coils)	0.5 cm.	70%
			1 cm.	65%
			1.5 cm.	60%
			2 cm.	55%
		Single layer with Ferro bar (x9 windingcoils + x9 Ferro-bars)	0.5 cm.	75%
			1 cm.	70%
			1.5 cm.	65%
			2 cm.	60%
Double side	Single layer (x12 magnets)	Single layer (x9 windingcoils)	0.5 cm.	80%
			1 cm.	76%
			1.5 cm.	65%
			2 cm.	55%

### System efficiency

The system efficiency was measured and resulted in Table 6, which was the efficiency of the receiver in electrical power. The generator, coupled to the DC motor, was tested at a speed of 700 rpm. The input power is the electrical power supplied to the motor driver. The output power is a difference in the air gaps, the ratio of output power against input power by voltage and current.

### Discussion

This article presents an innovative wireless power transmission system for marine applications. The system ensures safe power transmission from the transmitter to the receiver for charging purposes. The simulation results coincide with the experimental results. The proposed system differs from Conventional WPT systems because AC voltage is not required to be fed into the transmitter. The system can induce a voltage

in the receiver coil by rotating transmitters of a circular array of magnets.

### CONCLUSION

However, there is a difference in efficiencies obtained through simulation and experiments, as distance in real-time should be less to achieve better results than in a simulation environment. In the simulated environment, the air gap between the transmitters and receiver windings is selected in the 5-7 cm range, while in experiments, it varies from 0.5-2 cm. During simulation, the model was tested for three case scenarios: rotating only a single transmitter first, then rotating both transmitters simultaneously, and lastly varying the distance of each transmitter from the windings to determine the highest efficiency level. The highest voltage of 280 V was induced when both transmitters rotated, having an air gap of 5 cm from the receiver coil windings. Moreover, all the high

voltage ratings are achieved when both transmitters rotate regardless of the air gap. The induced voltage ratings in the receiver coil, while one of the transmitters is static, were comparatively low, with 89 V being the lowest. The experiments were then performed to test the results of the simulations. All three cases were repeated, and the highest possible efficiency (80%) was achieved in experiments when both transmitters moved. The proposed system is modeled and simulated in COMSOL and then tested by designing a prototype that shows promising results.

### ACKNOWLEDGMENTS

This research has been supported by the School of Engineering, Thammasat University. The authors would also like to thank Kruawan Wongpanya, Spectroscopic and Sensing Devices Research Group, NECTEC, Thailand Science Park, for providing access to the licensed version of COMSOL MULTIPHYSICS Software.

### REFERENCES

1. Vincent D, Sang PH, Williamson SS. Feasibility study of hybrid inductive and capacitive wireless power transfer for future transportation. 2017 IEEE Transportation Electrification Conference and Expo (ITEC), 2017 Jun 22-24; Chicago, IL, USA: IEEE; 2017.
2. Guo Y, Wang L, Zhang Y, Li S, Liao C. Rectifier load analysis for electric vehicle wireless charging system. IEEE Transactions on Industrial Electronics. 2018;65(9):6970-82.
3. Lu M. Synergetic Attenuation of Stray Magnetic Field in Inductive Power Transfer [dissertation]. Virginia: Virginia Polytechnic Institute; 2017.
4. Karimi S, Zadeh M, Suul JA. Shore charging for plug-in battery-powered ships: Power system architecture, infrastructure, and control. IEEE Electrification Magazine. 2020;8(3):47-61.
5. Wärtsilä's wireless charging: ahead of the game [Internet]. New York: 2017 - [updated 2017 Dec 4; cited 2020 Jun 9]. Available From: <https://www.shiptechnology.com/features/wartsilas-wireless-charging-ahead-game/>
6. Le K, Yuli HU, Wei Z. Maximum power efficiency tracking on underwater magnetic resonant wireless power transfer system. Journal of Harbin Engineering University. 2017;38:829-35.
7. Lin M, Li D, Yang C. Design of an ICPT system for battery charging applied to underwater docking systems. Ocean Engineering. 2017;145:373-81.
8. Yan Z, Zhang Y, Song B, Zhang K, Kan T, Mi C. An LCC-P compensated wireless power transfer system with a constant current output and reduced receiver size. Energies. 2019;12(1):172.
9. Kan T, Mai R, Mercier PP, Mi CC. Design and analysis of a three-phase wireless charging system for lightweight autonomous underwater vehicles. IEEE Transactions on Power Electronics. 2018;33(8):6622-32.
10. Yan Z, Zhang Y, Kan T, Lu F, Zhang K, Song B, et al. Frequency optimization of a loosely coupled underwater wireless power transfer system considering eddy current loss. IEEE Transactions on Industrial Electronics. 2019;66(5):3468-76.
11. Zhang K, Zhang X, Zhu Z, Yan Z, Member S, Song B, et al. A new coil structure to reduce eddy current loss of WPT systems for underwater vehicles. IEEE Transactions on Vehicular Technology. 2019; 68:245-53.
12. Lee IG, Kim N, Cho IK, Hong IP. Design of a patterned soft magnetic structure to reduce magnetic flux leakage of magnetic induction wireless power transfer systems. IEEE Transactions on Electromagnetic Compatibility. 2017;59:1856-63.
13. Yan Z, Song B, Zhang K, Wen H, Mao Z, Hu Y. Eddy current loss analysis of underwater wireless power transfer systems with misalignments. AIP Advances. 2018;8:101421.
14. Kan T, Zhang Y, Yan Z, Mercier PP, Mi CC. A rotation-resilient wireless charging system for lightweight autonomous underwater vehicles. IEEE Transactions on Vehicular Technology. 2018; 67(8):6935-42.
15. Tamura M, Naka Y, Murai K, Nakata T. Design of a capacitive wireless power transfer system for operation in fresh water. IEEE Transactions on Microwave Theory and Techniques. 2018;66(12): 5873-84.
16. Tamura M, Naka Y, Murai K. The design of a capacitive coupler for wireless power transfer under fresh water focuses on the kQ product. 2018 IEEE/ MTT-S International Microwave Symposium-IMS; 2018 Jun 10-15; Philadelphia, PA, USA: IEEE; 2018.
17. Urano M, Takahashi A. Study on underwater wireless power transfer via electric coupling. 2016 IEEE International Meeting for Future of Electron Devices, Kansai (IMFEDK); 2016 Jun 23-24; Kyoto, Japan: IEEE; 2016.

18. Sruthy V, Raj B, Preetha PK, Ilango K. SPV based Floating Charging Station with Hybrid Energy Storage. 2019 IEEE International Conference on Intelligent Techniques in Control, Optimization and Signal Processing (INCOS); 2019 Apr 11-13; Tamilnadu, India: IEEE; 2020.
19. Griffiths DJ. Introduction to electrodynamics. 3<sup>rd</sup> Ed. Upper Saddle River NJ: Prentice-Hall; 1999.
20. Sruthy V, Raj B, Preetha PK. An offshore floating charging station for electric ships: accessibility enhancement schemes for recharging. Ships and Offshore Structures. 2020;16(10):1143-50.